ON THE IMPACT OF ATMOSPHERIC THERMAL STABILITY ON THE CHARACTERISTICS OF NOCTURNAL DOWNSLOPE FLOWS

Z. J. YE[1], J. R. GARRATT[2], M. SEGAL and R. A. PIELKE

Department of Atmospheric Science, Colorado State University, Fort Collins, Colorado 80523, U.S.A.

(Received in final form 11 August, 1989)

Abstract. The impacts of background (or ambient) and local atmospheric thermal stabilities, and slope steepness, on nighttime thermally induced downslope flow in meso-β domains (i.e., 20–200 km horizontal extent) have been investigated using analytical and numerical model approaches. Good agreement between the analytical and numerical evaluations was found. It was concluded that: (i) as anticipated, the intensity of the downslope flow increases with increased slope steepness, although the depth of the downslope flow was found to be insensitive to slope steepness in the studied situations; (ii) the intensity of the downslope flow is generally independent of background atmospheric thermal stability; (iii) for given integrated nighttime cooling across the nocturnal boundary layer (NBL), Q_s, the local atmospheric thermal stability exerts a strong influence on downslope flow behavior: the downslope flow intensity increases when local atmospheric thermal stability increases; and (iv) the downslope flow intensity is proportional to $Q_s^{1/2}$.

. Introduction

The characteristics of thermally induced nocturnal downslope flows, referred to as drainage or katabatic flows, have been investigated extensively since Prandtl's (1942) well known study of valley flows. However, the impact of background atmospheric thermal stability (i.e., the atmospheric thermal stability around sunset; defined as $\beta_0 = \mathrm{d}\theta_0/\mathrm{d}z$, where θ_0 is the background potential temperature) and local atmospheric thermal stability (defined as $\gamma = \mathrm{d}\theta/\mathrm{d}z$, where θ is the local atmospheric potential temperature) on nocturnal downslope flows along meso-β slopes has been given little attention due to a lack of suitable data. The background thermal stability following a synoptically unperturbed clear day is usually close to neutral. However, when the area is affected by a thermally stable air mass (e.g., as a result of an intense high pressure system with strong subsidence, or penetration of an arctic air mass to the mid-latitudes), the background thermal stability, β_0, may deviate considerably from the neutral thermal stratification.

For short slopes, Ellison and Turner (1959), and Manins and Sawford (1979a, b) indicated that downslope flow is strongly influenced by entrainment caused by turbulent mixing and convergence. The latter was supported by the Doran and Horst (1983) observational data analysis. Nappo and Rao (1987) devoted some attention to evaluating the impact of β_0 on downslope flow, along very short

[1] Permanent address: Institute of Atmospheric Physics, Academia Sinica, Beijing, China.
[2] Permanent address: CSIRO, Division of Atmospheric Research, Victoria, Australia.

Boundary-Layer Meteorology **51**: 77–97, 1990.

slopes, using a two-dimensional (2-D) numerical model. They found that only for short distances from the slope crest ($\leqslant 1000$ m) did the background atmospheric thermal stability, β_0, profoundly affect the flow structure by modifying its depth and speed. Additionally, they showed that as the thermal stratification increases, the flow approaches the one-dimensional case in a shorter distance from the crest, and that as this case was reached, the entrainment vanished.

The role of background and local atmospheric thermal stability upon thermally induced meso-β scale downslope flows requires additional clarification. Resolution of this problem is needed since the characteristics of these flows have importance in environmental problems as well as in weather forecasting

It is the purpose of the present study to provide an additional exploration of the impact of β_0 and γ on the development of downslope flows utilizing analytical and numerical modeling approaches. The evaluations in the present study assume a negligible synoptic flow, in order to isolate that impact. Slope lengths on the order of 100 km, which are typical of large meso-β domains, are considered. The analytical approach (Section 2) includes several refinements to improve the solutions obtained in previous analytical modeling studies. The numerical model (Section 3) provides simulated fields for evaluating the analytical results.

2. Analytical Methodology

In this section, the mathematical formulation associated with the analytical model evaluations is described. This involves some refinements designed to improve the realism of the major physical processes related to downslope flows. Special emphasis is given to the scaling of the eddy exchange coefficient. Since the buoyancy force across the nocturnal boundary layer (NBL) is the major physical forcing of the nocturnal downslope flow, the impact of β_0 and the local atmospheric thermal stabililty, γ, (i.e., the one forced by local diabatic cooling) on downslope flow is studied while assuming that the buoyancy force across the NBL remains unchanged.

2.1. A DIAGNOSTIC EQUATION FOR θ'; THE DEPARTURE OF POTENTIAL TEMPERATURE ABOVE THE SLOPE FROM THE AMBIENT POTENTIAL TEMPERATURE

The potential temperature conservation equation above a long homogeneous slope in unsteady conditions and without synoptic flow can be written as:

$$\frac{\partial \theta'}{\partial t} - u' \beta_0 \sin \alpha = -\frac{\partial H_s}{\partial z} + \frac{1}{\rho c_p} \frac{\partial R_N}{\partial z} \tag{1}$$

where z is the vertical coordinate perpendicular to the slope, u' is the slope flow intensity (positive in the downslope direction), θ' is the departure of potential temperature θ above the slope from the ambient potential temperature, θ_0, at the

same level, α is the slope inclination angle, $H_s = -K\,\partial\theta'/\partial z$ is the vertical turbulent flux of heat, ρ is the density of the air, and c_p is the specific heat of air at constant pressure, $R_N = R\downarrow - R\uparrow$ is the net long-wave radiative (LWR) flux. Here $R\uparrow$ and $R\downarrow$ are the upward and downward LWR fluxes, respectively, where R_N is known to be a complex function of atmospheric temperature, water vapor and aerosol content, and soil components (e.g., soil wetness, soil type) which determine the atmospheric and ground surface emissivities and irradiance characteristics.

The presence of nonlinear terms involved with the evaluation of the LWR flux divergence prevents a simplified analytical solution for Equation (1); some authors have even neglected the LWR flux divergence term (e.g., Rao and Snodgrass, 1981; Kondo, 1984). However, in order to overcome this limitation, a diagnostic equation of θ can be established which is based upon observational data for θ, and so, indirectly, includes the contributions from long-wave radiative flux divergence terms to θ. The profile form of θ (see illustration in Figure 1) is given by

$$\theta = \theta_h - \Delta\theta f(\xi)\,, \tag{2a}$$

where $\xi = z/h$ is a nondimensional height related to the depth of the NBL, h; θ_h is the potential temperature at $\xi = 1$; and $\Delta\theta = \theta_h - \theta_s$ (defining the surface inversion intensity), where θ_s is the value of θ at the surface. The functional relation $f(\xi)$ is assumed to be given by:

$$f(\xi) = (1 - \xi)^n$$

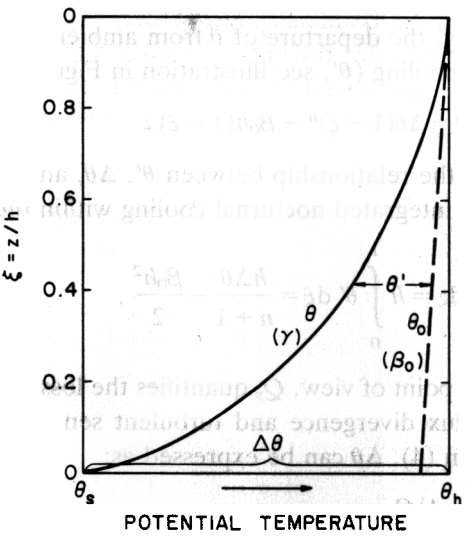

Fig. 1. Schematic illustration of the thermal variables θ_h, θ, θ_0, θ', and θ_s which are related through Equations (2–4).

and the local atmospheric thermal stability is, therefore,

$$\gamma = \frac{d\theta}{dz} = \frac{\Delta\theta}{h} n(1-\xi)^{n-1} \tag{2c}$$

The value of n is apparently strongly dependent on the relative contributions of radiative and turbulent cooling across the NBL as discussed by André and Mahrt (1982) and more recently by Garratt and Ryan (1989). The NBL observational and numerical model results over flat terrain show that potential temperature profiles of significant positive curvature (i.e., convex to the surface; $n>1$) (e.g., André and Mahrt, 1982) occur when radiative cooling within the NBL dominates (e.g., the Wangara conditions). Yamada (1979) presented an empirical expression for $f(\xi)$, giving $n=3$ based on the Wangara data analysis. In Dickerson (1980), a potential temperature profile presented for the PDC-1 site at Cobb Mountain, California, as well as numerical modeling results, suggested that the basic function $f(\xi)$ would have to be cubic. In contrast, profile forms of θ when turbulent cooling dominates (observations and model results) have significant negative profile curvature (i.e., concave to the surface) with $n \rightarrow 0.5$ (André and Mahrt, 1982; Garratt and Ryan, 1989). For slope flows, Yasuda *et al.* (1986) presented θ profiles with a linear increase with height (i.e., with $n=1$) observed in a V-shaped valley in Japan. In these cases, the relative contributions by turbulent and net radiative divergence cooling to the total nocturnal cooling within the NBL are assumed to be approximately equal. Equation (2c) indicates that with $n>1$, the magnitude of γ decreases with increasing height, and with $n<1$, it increases, i.e., radiative cooling acts to reduce the magnitude of γ in the upper part of the NBL (as presented by André and Mahrt, 1982) and turbulent heat exchange tends to decrease it in the lower part of the NBL.

In the present study, the departure of θ from ambient potential temperature as a result of nocturnal cooling (θ', see illustration in Figure 1) is approximated by:

$$\theta' = \theta_0 - \theta \simeq \Delta\theta(1-\xi)^n - \beta_0 h(1-\xi)\,. \tag{3}$$

Equation (3) defines the relationship between θ', $\Delta\theta$, and β_0.

Defining Q_s as the integrated nocturnal cooling within the NBL:

$$Q_s = \int_0^h \theta'\,dz = h\int_0^1 \theta'\,d\xi = \frac{h\Delta\theta}{n+1} - \frac{\beta_0 h^2}{2} \tag{4}$$

then, from a physical point of view, Q_s quantifies the loss of thermal energy within the NBL by LWR flux divergence and turbulent sensible heat flux divergence. Rearranging Equation (4), $\Delta\theta$ can be expressed as:

$$\Delta\theta = \frac{A(n+1)Q_s}{h}\,, \tag{5a}$$

where

$$A = \left[\frac{\beta_0 h^2}{2Q_s} \right.$$

Equation (5a) indicates that the surface inversion intensity, $\Delta\theta$, increases with increasing values of Q_s and/or n. Substituting Equation (5a) into Equation (2c) results in:

$$\gamma = \frac{An(n+1)Q_s}{h^2}(1-\xi)^{n-1} \tag{6a}$$

which indicates that the local atmospheric thermal stability, γ, increases with increasing values of n for constant Q_s. Therefore, n can be viewed as an index dependent on the local atmospheric thermal stability magnitude, or the surface inversion intensity. The magnitude of γ becomes greater as Q_s increases (Equation 6a) or as $\Delta\theta$ increases (Equations 5a and 6a) with fixed n. Substituting Equation (5a) into (3) results in:

$$\theta' = \frac{Q_s}{h}\left[A(n+1)(1 \quad \xi)^{(n-1)} - \frac{\beta_0 h^2}{Q_s} \right. (1 \quad \xi)$$

Equation (6b) provides a relation between θ' and β_0, h, n, ξ and Q_s which is used in the derivations in the next subsection.

2.2. The dependence of downslope flow on β_0, Q_s and slope angle

In most practical cases, the nocturnal downslope flow reaches nearly a steady state several hours following sunset (this is supported by both observations and modeling studies; in the 2-D numerical simulations presented in Section 3, the required time for steady state is about 6 hours). Therefore, the properties of steady-state flow are of general interest. This subsection focuses on the structure of a steady downslope flow situation. In the following derivation of the nocturnal downslope flow, u', we assume that the vertical profile of θ' can be determined using Equation (6b).

Assuming that the downslope flow component, u', does not vary along the middle of a long slope and that the Coriolis force effect can be neglected in a shallow NBL, then the steady equation of the x-component (parallel to the slope) of momentum for the downslope flow is (e.g., Prandtl, 1942)

$$\frac{\partial}{\partial\xi}\left(K\frac{\partial u'}{\partial\xi}\right) + h^2\lambda\theta' \sin\alpha = 0 \tag{7}$$

where $\lambda = g/\theta$.

Equation (7) is solved within a NBL with a given depth, h, while assuming a scaled K based on derivations in the Appendix, which is dependent on thermal

stability through the relation

$$K = K_0 h \left(\frac{Q_s}{n}\right)^{1/2} \tag{8}$$

where K_0 is a constant with units in $m^{1/2} K^{-1/2} s^{-1}$ (see the Appendix for details and its definition).

The solution of Equation (7) using K as defined by Equation (8), and assuming the boundary conditions $u' = 0$ at $\xi = 0$, 1 [i.e., assuming that, as a first approximation, the NBL depths as determined from both the downslope flow profile and the potential temperature profile are equal (e.g., Table 2, Yasuda *et al.*, 1986)] is:

$$u' = \frac{Q_s^{1/2} \lambda \sin \alpha}{K_0} \cdot \eta ,$$

where

$$\eta = n^{1/2} \left\{ \frac{A}{(n+2)} [1 - (1-\xi)^{n+1}] - \frac{\beta_0 h^2}{6 Q_s} \xi (2 - \xi) \right\} \quad (1-\xi)$$

Equation (9a) suggests that, (a) u' is proportional to $Q_s^{1/2}$; and (b) u' is proportional to $\sin \alpha$ when the value of n is kept unchanged. However, as u' increases with steepness, the sensible heat flux and turbulent exchange coefficient increase too, resulting in some decrease in the value of n. Thus, u' should deviate somewhat from the linear dependence on $\sin \alpha$ (as supported by the numerical result in Section 3.2), unless the value of n is appropriately adjusted. From Equation (5a), the surface inversion intensity, $\Delta\theta$, increases with increasing values of n and Q_s. As discussed above, the downslope flow is proportional to $Q_s^{1/2}$; thus, the downslope flow is proportional to $(\Delta\theta)^{1/2}$ for the same value of n.

The dependence of the downslope flow intensity, u', on the local atmospheric stability index, n, as indicated by η, is illustrated in Figure 2a. The figure suggests that for the same values of Q_s, $\sin \alpha$, and K_0, when n increases (which implies an increase of γ; see Equation 2c; however, it is assumed that cases with $n > 1$ reflect fairly extreme situations, as the slope steepness increases), the value of η and correspondingly the value of u' increase and the height of the maximum value of η decreases. As discussed in sub-section (2.1), when the value of n increases, the contribution of the LWR flux divergence to nocturnal cooling within the NBL increases; when the value of n decreases, the contribution of sensible heat flux divergence to Q_s increases. Therefore Figure 2a indicates that for a fixed value of Q_s, stronger downslope flow will result from an increase in the contribution of LWR flux divergence to Q_s. Figure 2b illustrates the impact of variation in n on the profile of $\theta - \theta_h$, and indicates that for the same values of Q_s and β_0, the surface inversion intensity and the value of θ' near the surface increases with increasing n. Therefore, the relation between u' and n can be explained as follows:

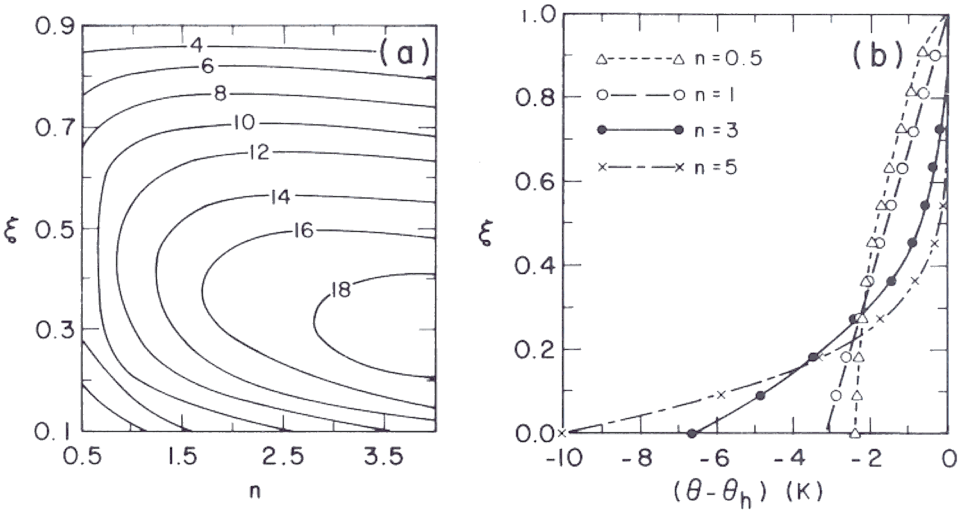

Fig. 2. (a) The dependence of η on n and ξ (see Equation 9b), for a moderate value of $Q_s = 157$ m K, and with $h = 114$ m and $\beta_0 = 1$ K km^{-1}; (b) the impact of a variation in n on the θ profile, based on Equation (6b), and using the same parameters as in (a).

for fixed Q_s, when the index n increases, according to Equation (5a), the nocturnal surface inversion intensity ($\Delta\theta$) increases. Also the perturbation potential temperature, θ', increases in the lower part of NBL as expressed by Equation (6b) and indicated by Figure 2b. Therefore, the buoyancy force as expressed by the second term in Equation (7) increases in the lower part of the NBL. On the other hand, the value of the eddy exchange coefficient decreases with increasing n as indicated by Equation (8), since the value of γ tends then to be greater [see Equation (2c)]. The more stable atmosphere corresponds to smaller eddy exchange coefficients. Based on Equation (7), and the aforementioned features, increasing n results in larger values of $\partial u'/\partial\xi$ in order to increase the turbulent friction force needed to balance the increased buoyancy force.

In order to isolate the effect of β_0 on u', using equations (5b) and (6a), equations (9a, b) were rewritten as:

$$u' = \frac{(nQ_s)^{1/2}\lambda \sin\alpha}{(n+2)K_0}[1-(1-\xi)^{n+1}](1-\xi)\left(1+\eta^*\frac{\beta_0}{\gamma^*}\right),$$

where

$$\gamma^* = \frac{n(n+1)Q_s}{h^2}(1-\xi)^{n-2}\left[1-\frac{(2+n)}{3}\frac{\xi(2-\xi)}{(1-(1-\xi)^{n+1})}\right]$$

stability through the relation

$$K = K_0 h \left(\frac{Q_s}{n}\right)^{1/2} \tag{8}$$

where K_0 is a constant with units in $m^{1/2} K^{-1/2} s^{-1}$ (see the Appendix for details and its definition).

The solution of Equation (7) using K as defined by Equation (8), and assuming the boundary conditions $u' = 0$ at $\xi = 0$, 1 [i.e., assuming that, as a first approximation, the NBL depths as determined from both the downslope flow profile and the potential temperature profile are equal (e.g., Table 2, Yasuda *et al.*, 1986)] is:

$$u' = \frac{Q_s^{1/2} \lambda \sin \alpha}{K_0} \eta,$$

where

$$\eta = n^{1/2} \left\{ \frac{A}{(n+2)} [1 - (1-\xi)^{n+1}] - \frac{\beta_0 h^2}{6 Q_s} \xi (2 - \xi) \right\} (1-\xi).$$

Equation (9a) suggests that, (a) u' is proportional to $Q_s^{1/2}$; and (b) u' is proportional to $\sin \alpha$ when the value of n is kept unchanged. However, as u' increases with steepness, the sensible heat flux and turbulent exchange coefficient increase too, resulting in some decrease in the value of n. Thus, u' should deviate somewhat from the linear dependence on $\sin \alpha$ (as supported by the numerical result in Section 3.2), unless the value of n is appropriately adjusted. From Equation (5a), the surface inversion intensity, $\Delta\theta$, increases with increasing values of n and Q_s. As discussed above, the downslope flow is proportional to $Q_s^{1/2}$; thus, the downslope flow is proportional to $(\Delta\theta)^{1/2}$ for the same value of n.

The dependence of the downslope flow intensity, u', on the local atmospheric stability index, n, as indicated by η, is illustrated in Figure 2a. The figure suggests that for the same values of Q_s, $\sin \alpha$, and K_0, when n increases (which implies an increase of γ; see Equation 2c; however, it is assumed that cases with $n > 1$ reflect fairly extreme situations, as the slope steepness increases), the value of η and correspondingly the value of u' increase and the height of the maximum value of η decreases. As discussed in sub-section (2.1), when the value of n increases, the contribution of the LWR flux divergence to nocturnal cooling within the NBL increases; when the value of n decreases, the contribution of sensible heat flux divergence to Q_s increases. Therefore Figure 2a indicates that for a fixed value of Q_s, stronger downslope flow will result from an increase in the contribution of LWR flux divergence to Q_s. Figure 2b illustrates the impact of variation in n on the profile of $\theta - \theta_h$, and indicates that for the same values of Q_s and β_0, the surface inversion intensity and the value of θ' near the surface increases with increasing n. Therefore, the relation between u' and n can be explained as follows:

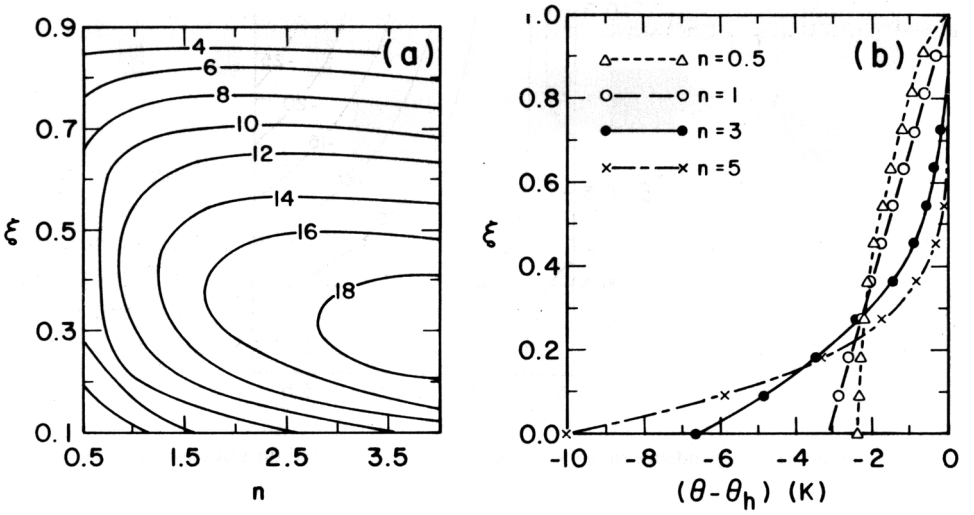

Fig. 2. (a) The dependence of η on n and ξ (see Equation 9b), for a moderate value of $Q_s = 157$ m K, and with $h = 114$ m and $\beta_0 = 1$ K km^{-1}; (b) the impact of a variation in n on the θ profile, based on Equation (6b), and using the same parameters as in (a).

for fixed Q_s, when the index n increases, according to Equation (5a), the nocturnal surface inversion intensity ($\Delta\theta$) increases. Also the perturbation potential temperature, θ', increases in the lower part of NBL as expressed by Equation (6b) and indicated by Figure 2b. Therefore, the buoyancy force as expressed by the second term in Equation (7) increases in the lower part of the NBL. On the other hand, the value of the eddy exchange coefficient decreases with increasing n as indicated by Equation (8), since the value of γ tends then to be greater [see Equation (2c)]. The more stable atmosphere corresponds to smaller eddy exchange coefficients. Based on Equation (7), and the aforementioned features, increasing n results in larger values of $\partial u'/\partial\xi$ in order to increase the turbulent friction force needed to balance the increased buoyancy force.

In order to isolate the effect of β_0 on u', using equations (5b) and (6a), equations (9a, b) were rewritten as:

$$u' = \frac{(nQ_s)^{1/2}\lambda \sin\alpha}{(n+2)K_0}[1-(1-\xi)^{n+1}](1-\xi)\left(1+\eta^*\frac{\beta_0}{\gamma^*}\right),$$

where

$$\eta^* = \frac{n(n+1)}{2}(1-\xi)^{n-1}\left[1 \quad \frac{(2+n)}{} \quad \frac{\xi(2-\xi)}{}\right]$$

$$\gamma^* = \frac{n(n+1)Q_s}{h^2}(1-\xi)^{n-1}$$

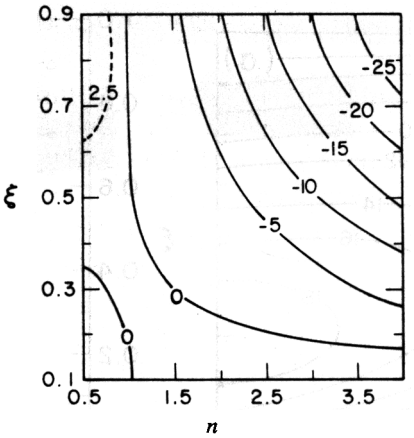

Fig. 3. The dependence of η^*/γ^* (m K^{-1}) on n and ξ, based on Equation (10b, c).

As implied by Equations (5b), (6a), and (10c), except for extremely weak NBL cooling (i.e., very small Q_s values), $\gamma^* \approx \gamma$.

The factor $\eta^*(\beta_0/\gamma^*)$ in Equation (10a) indicates the relative importance of γ and β_0 on the downslope flow speed, u'. It is evident from Equation (10a) that when $(\eta^*/\gamma^*)\beta_0 \ll 1$, the impact of β_0 on u' is negligible. Figure 3 provides a nomogram of η^*/γ^* as a function of ξ and n. It indicates that the absolute value of η^*/γ^* increases with increasing n and ξ. Based on Figure 3, for commonly observed values of β_0 (i.e., $\sim[10^{-3}]$ K m^{-1}), $|(\eta^*/\gamma^*)\beta_0| \ll 1$. On the other hand, for extremely high values of β_0 (i.e., $\sim[10^{-2}]$ K m^{-1}), $|(\eta^*/\gamma^*)\beta_0|$ can reach 0.1 to 0.25 when $n > 3$ and $\xi > 0.5$. However, even in these situations the impact of β_0 on u' would seem to be insignificant. In conclusion, Equations (9a–b) and Equations (10a–c) suggest that the thermally induced downslope flow is independent of the initial background atmospheric thermal stability, β_0. However, the flow is influenced by the local atmospheric thermal stability, γ, within the NBL which evolves along with the downslope flow. Increasing γ by increasing the values of n and/or Q_s based on Equation (6a), results in an increase of the downslope flow intensity. The non-dimensional height at which the downslope flow reaches its maximum value decreases when increasing the value of the stratification index n.

3. Numerical Model Simulations

In order to assess the analytical results, a set of numerical model simulations (see Table I for their general description) designed to evaluate the impact of β_o, and the local atmospheric stratification, on the thermally induced downslope flow at night for steady and unsteady conditions were carried out. A 2-D hydrostatic primitive equation numerical model was used, where its formulation is given in

detail in Pielke (1974), Mahrer and Pielke (1977), and McNider and Pielke (1981) and is not repeated here.

The vertical domain of the model ranges from the surface to 15 km (the model levels for potential temperature and specific humidity, and related initial values below $z = 1750$ m, are given in Table II). The simulated domain extends horizontally for 240 km, consisting of a flat-slope-plateau terrain configuration (the slope area extended horizontally for 100 km), and with a horizontal grid interval of 5 km. The model input parameters are given in Table III. The numerical model used in the present study was applied successfully to simulate slope flows in case studies (e.g., McNider and Pielke (1981, 1984); Segal *et al.* (1982), among others). Since the slope is long enough, the contribution of the non-linear terms and entrainment effects should be relatively small along most of the slope.

TABLE I

Brief description of the numerical model simulations

Case 1	Steady state numerical model simulations (potential temperature is prescribed); sensitivity of the downslope flow to atmospheric background thermal stability ($\beta_0 = 1$ and $10\ \mathrm{K\ km^{-1}}$), and stability index n ($n = 1$ and 3), $h = 125$ m and $Q_s = 252$ m K. Slope followed by plateau with height of $H = 500$ m ($\alpha = 0.28°$)
Case 2	Time-dependent simulations, sensitivity of downslope flow to the atmospheric background thermal stability and slope steepness, with $\beta_0 = 1\ \mathrm{K\ km^{-1}}$ and $10\ \mathrm{K\ km^{-1}}$. Slope followed by plateau with heights of (a) $H = 250$ m ($\alpha = 0.14°$); (b) $H = 500$ m ($\alpha = 0.28°$); (c) $H = 1000$ m ($\alpha = 0.57°$).

TABLE II

The numerical model levels for potential temperature and specific humidity (in the lower 1750 m of the atmosphere) and the related values

	Level (m)														
			15	30	55	85	125	175	250	400	600	800	1050	1350	1750
q(g kg^{-1})	3.16	3.15	3.14	3.12	3.08	3.04	2.98	2.90	2.79	2.50	2.20	1.90	1.48	0.79	0.40
θ (K)	280.0	Specified according to the given value of β_0													

TABLE III

The model input parameters used in the numerical model simulations

Surface Albedo	Surface roughness (m)	Soil diffusivity ($\mathrm{m^2\ s^{-1}}$)	Soil density ($\mathrm{kg\ m^{-3}}$)	Soil specific heat ($\mathrm{J\ kg^{-1}\ K^{-1}}$)	Latitude (deg)	Day	Time step interval (Δt) (s)	Horizontal grid interval (Δx) (km)
0.2	0.04	3×10^{-7}	1500	1330	32	21 December	45	5

In the present study, the numerical model was applied in two modes: steady and unsteady state. In the steady mode, a prescribed potential temperature, θ, profile was used, which is kept unchanged while integrating the model to steady state. Using this approach, enables the introduction of potential temperature profiles based on Equation (6b), and a straightforward comparison of the numerically simulated flow with the flow computed by the analytical approach. The numerical model provides a close duplication of the analytical model, yet includes considerably more detailed physical processes. Thus, the comparison enables an evaluation of the solutions obtained by the analytical model. In addition, unsteady model similations were carried out, and an essentially steady state was reached after several hours of integration.

3.1. Steady state 2-D simulations

In the steady state 2-D simulations (see Case 1; Table I), moderate values of NBL height h, and the total cooling in the NBL, Q_s (as defined by Equation 4), were prescribed as follows: $h = 125$ m and $Q_s = 252$ m K. Based on these values and Equation (6b), the potential temperature perturbation θ' was computed using $n = 1$ and 3, and $\beta_0 = 1$ and 10 K km^{-1}, replacing the model prediction equation for θ'. With this prescribed θ', the model was integrated until nearly steady state downslope flow was established.

Case 1 was designed to illustrate the impact of a change of β_0 over a wide range from a background atmospheric thermal stability of nearly neutral ($\beta_0 = 1$ K km^{-1}) to β_0 representing a very stable condition ($\beta_0 = 10$ K km^{-1}) in order to simulate the possible impact of β_0 on downslope flow. The computed results shown in

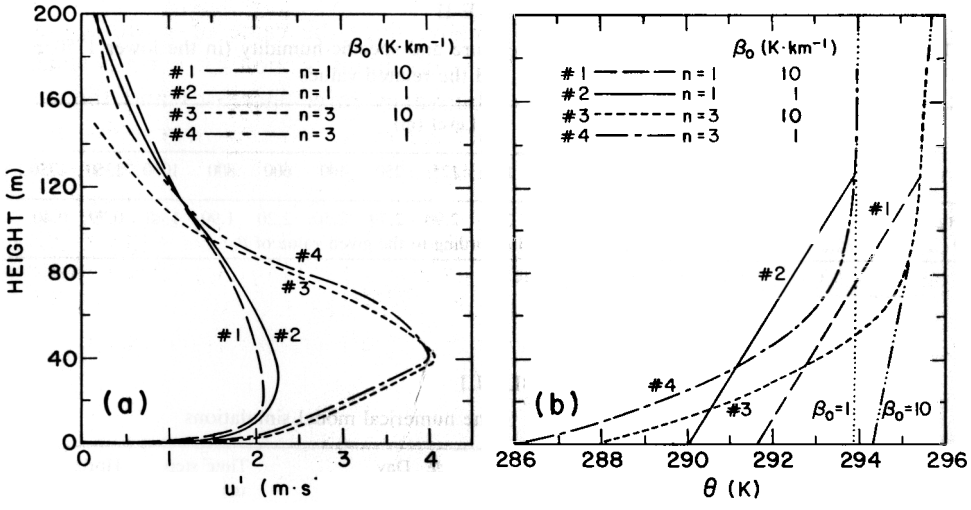

Fig. 4. Numerical model simulated vertical profiles of downslope flow at the middle of the slope (Case 1): with $Q_s = 252$ m K, $h = 125$ m (a) downslope wind profiles under steady situations, showing the impact of various β_0 and n values (as indicated) on the downslope flow intensity. (b) potential temperature profiles prescribed for the situation presented in (a).

Figure 4a indicate that the downslope wind profiles computed for both stabilities and for $n = 1$ and 3, respectively, are nearly the same. The depth of downslope flow seems independent of β_0 for the chosen values of n. These results for the steady 2-D numerical simulations are in agreement with those for the analytical solution (as was implied by Figure 3). Therefore, the results from the simulations in Case 1 provide further evidence to support the conclusion that the downslope flow is generally insensitive to β_0 (as will be shown in subsection 3.2 (Figure 5), this condition is closely fulfilled also in the unsteady simulations). It should be emphasized that this conclusion drawn from Case 1 assumes that the integrated cooling within the NBL retains the same value, as the value of β_0 is changed.

As discussed in Section 2, the value of the local atmospheric thermal stability, γ, can be changed by changing values of n, h, or Q_s: the value of γ increases by increasing the values of n and/or Q_s and decreasing h, leading to an increase in the downslope flow intensity. However, our emphasis is in evaluating the impact of γ on downslope flow structure under the condition that Q_s is fixed. Case 1 was also designed to investigate the impact of γ as expressed through different values of n on downslope flow intensity under the constraint that Q_s, β_0, and α were kept unchanged. The downslope wind intensity (see Figure 4a) forced by the same Q_s, is dependent on the values of n, as illustrated by changing the value of n from $n = 1$ to $n = 3$. Both the surface inversion intensity and the downslope wind speed in the lower parts of the NBL increase with n; where the maximum downslope wind speed for $n = 3$ is about 1.9 times as large as that for $n = 1$ for both values of β_0. However, in the upper part of the NBL, the downslope wind intensity for $n = 1$ and 3 shows less pronounced differences. The reason for these profile features is that the potential temperature perturbation with $n = 3$ is larger (and consequently the buoyancy force is also larger) in the lower parts of NBL than that with $n = 1$ (see Figure 4b). Additionally, since the value of γ with $n = 3$ is larger than that corresponding to $n = 1$, the turbulent friction for $n = 3$ is smaller than that with $n = 1$. As a result, the buoyancy force increases and the eddy exchange coefficient decreases with an increase in the value of n, resulting in an increase of downslope flow intensity. In the upper part of the NBL, the situation is reversed.

In conclusion, the results gained from the 2-D steady-state simulations suggest that the downslope flow forced by the same integrated buoyancy force is almost independent of the value of β_0, but the flow is profoundly affected by γ. The maximum downslope flow intensity increases as the value of n is increased.

3.2. Unsteady 2-D model simulations

In the previous subsection, the investigation of the impact of β_0 and n on the thermally induced downslope flow intensity concentrated on the steady-state condition. In the following time dependent integrations (i.e., involved with a prediction equation for θ'), model simulations through the nocturnal period are considered. Simulation results are compared against those obtained from the analytical solution and the numerical simulations under the steady-state constraint.

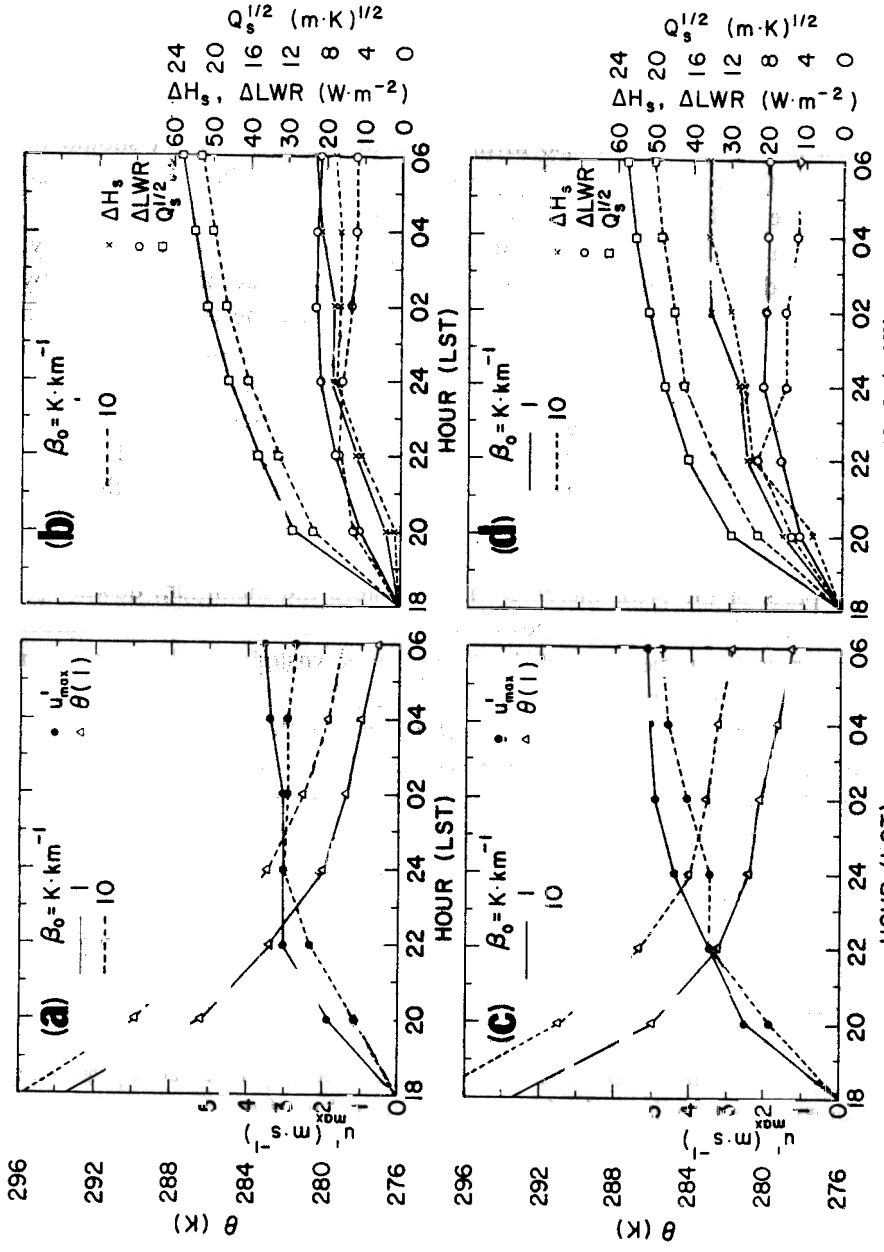

Fig. 5. Time dependent variations of u'_{max}, $\theta(1)$, Q_s, ΔH_s, and ΔLWR at the middle of the slope for $\beta_0 = 1$ K km^{-1} and $\beta_0 = 10$ K km^{-1}, as obtained from 2-D simulations (Case 2). (a, b) $H = 250$ m; $\alpha = 0.14°$; (c, d) $H = 500$ m; $\alpha = 0.28°$; (e, f) $H = 1000$ m; $\alpha = 0.57°$.

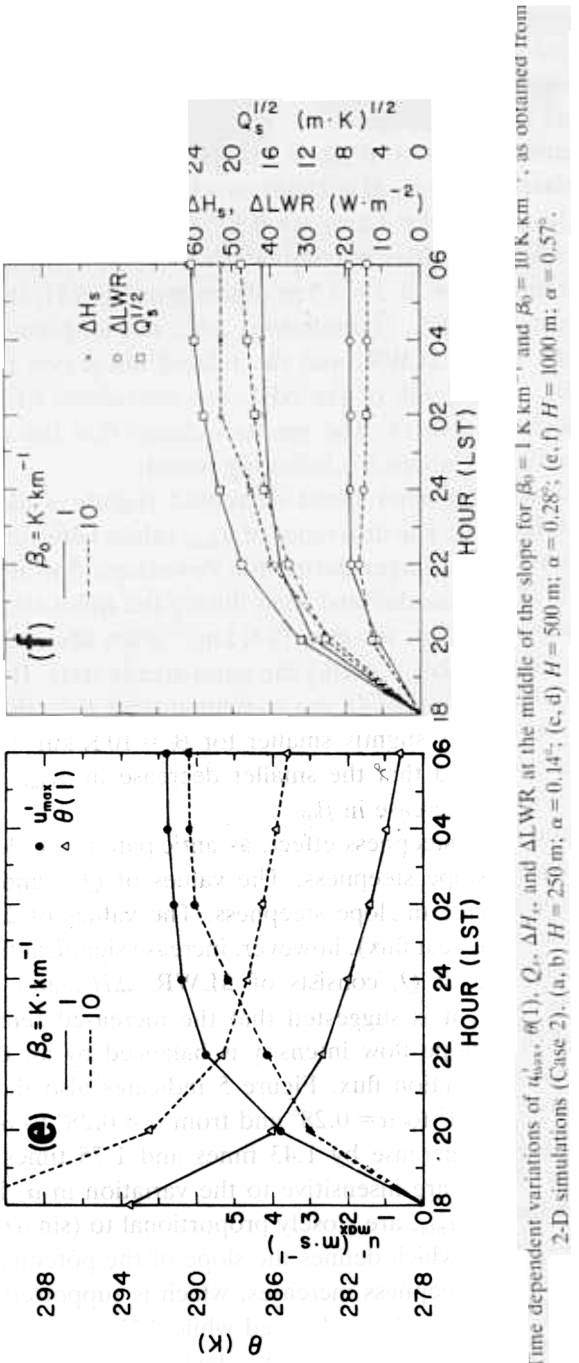

Fig. 5. Time dependent variations of u'_{max}, $\theta(1)$, Q_s, ΔH_s, and ΔLWR at the middle of the slope for $\beta_0 = 1$ K km^{-1} and $\beta_0 = 10$ K km^{-1}, as obtained from 2-D simulations (Case 2). (a, b) $H = 250$ m; $\alpha = 0.14°$; (c, d) $H = 500$ m; $\alpha = 0.28°$; (e, f) $H = 1000$ m; $\alpha = 0.57°$.

Case 2 was designed to investigate the sensitivity of thermally induced downslope flow to the value of β_0, using two extreme stabilities ($\beta_0 = 1\ \mathrm{K\ km^{-1}}$ and $\beta_0 = 10\ \mathrm{K\ km^{-1}}$) for illustration. Case 2 was also designed to provide additional information on the effect of slope steepness.

Figure 5 represents the impact of β_0 on several quantities in the middle of the slope for several plateau heights: $H = 250$ m; $\alpha = 0.14°$ (Figure 5a–b), $H = 500$ m; $\alpha = 0.28°$ (Figure 5c–d) and $H = 1$ km; $\alpha = 0.57°$ (Figure 5e–f). The time dependence of the following quantities is considered: the maximum downslope wind $u'_{\max}$; surface air temperature at $z = 3.5$ m above ground $\theta(1)$; the sensible heat flux difference across the NBL, (bottom-top) ΔH_s; net long-wave radiative flux difference across the NBL, ΔLWR, and the related integrated buoyancy force, $Q_s^{1/2}$ within the NBL. The depth of the NBL was considered to be the same as that of the downslope flow layer. The results indicate that the downslope flow reaches a quasi-steady state about 6 h following sunset.

The maximum downslope wind speed decreased slightly while increasing β_0 from $1\ \mathrm{K\ km^{-1}}$ to $10\ \mathrm{K\ km^{-1}}$. The difference of $u'_{\max}$ values between $\beta_0 = 1\ \mathrm{K\ km^{-1}}$ and $10\ \mathrm{K\ km^{-1}}$ was relatively larger during the downslope flow developing stage (i.e., in the first 6 h of the simulations) than during the quasi-steady conditions. The maximum downslope winds for $\beta_0 = 10\ \mathrm{K\ km^{-1}}$ were about 0.8 to 0.9 times as strong as that for $\beta_0 = 1\ \mathrm{K\ km^{-1}}$ during the quasi-steady state. It is evident from Figure 5 that $Q_s^{1/2}$ (where values of Q_s are computed from Equation (4) using the simulated θ values) were only slightly smaller for $\beta_0 = 10\ \mathrm{K\ km^{-1}}$ than those for $\beta_0 = 1\ \mathrm{K\ km^{-1}}$. It is suggested that the smaller decrease in $u'_{\max}$ corresponds to a reduction in $Q_s^{1/2}$ with an increase in β_0.

With regards to the slope steepness effect, as anticipated, the downslope wind increases with increasing slope steepness. The values of $Q_s^{1/2}$ and ΔLWR show little sensitivity to the change in slope steepness. The values of ΔH_s (which are equal to the surface sensible heat flux), however, increase significantly with increasing slope. Since the value of Q_s consists of ΔLWR, ΔH_s, and the total heat advection within the NBL, it is suggested that the increased sensible heat flux caused by increased downslope flow intensity is balanced by an increase in the downslope temperature advection flux. Figure 5 indicates also that doubling of slope steepness from $\alpha = 0.14°$ to $\alpha = 0.28°$ and from $\alpha = 0.28°$ to $\alpha = 0.57°$ produces a corresponding $u'_{\max}$ increase by 1.43 times and 1.75 times, respectively. However, the values of $Q_s^{1/2}$ are insensitive to the variation in α. It is suggested that the simulated values of $u'_{\max}$ are closely proportional to $(\sin \alpha)^{1/2}$. This result suggests that the value of n, which defines the slope of the potential temperature profile, should decrease as steepness increases, which is supported by Figure 5;' when α increases, ALWR is nearly unchanged while ΔH, increases significantly. This explains why the downslope flow intensity deviates from the proportionality to $\sin \alpha$ as suggested by Equation (9a). In addition, it suggests that, for a dry shallow nocturnal downslope flow evolving over a slope of more than a few degrees inclination, the net radiation flux may be neglected.

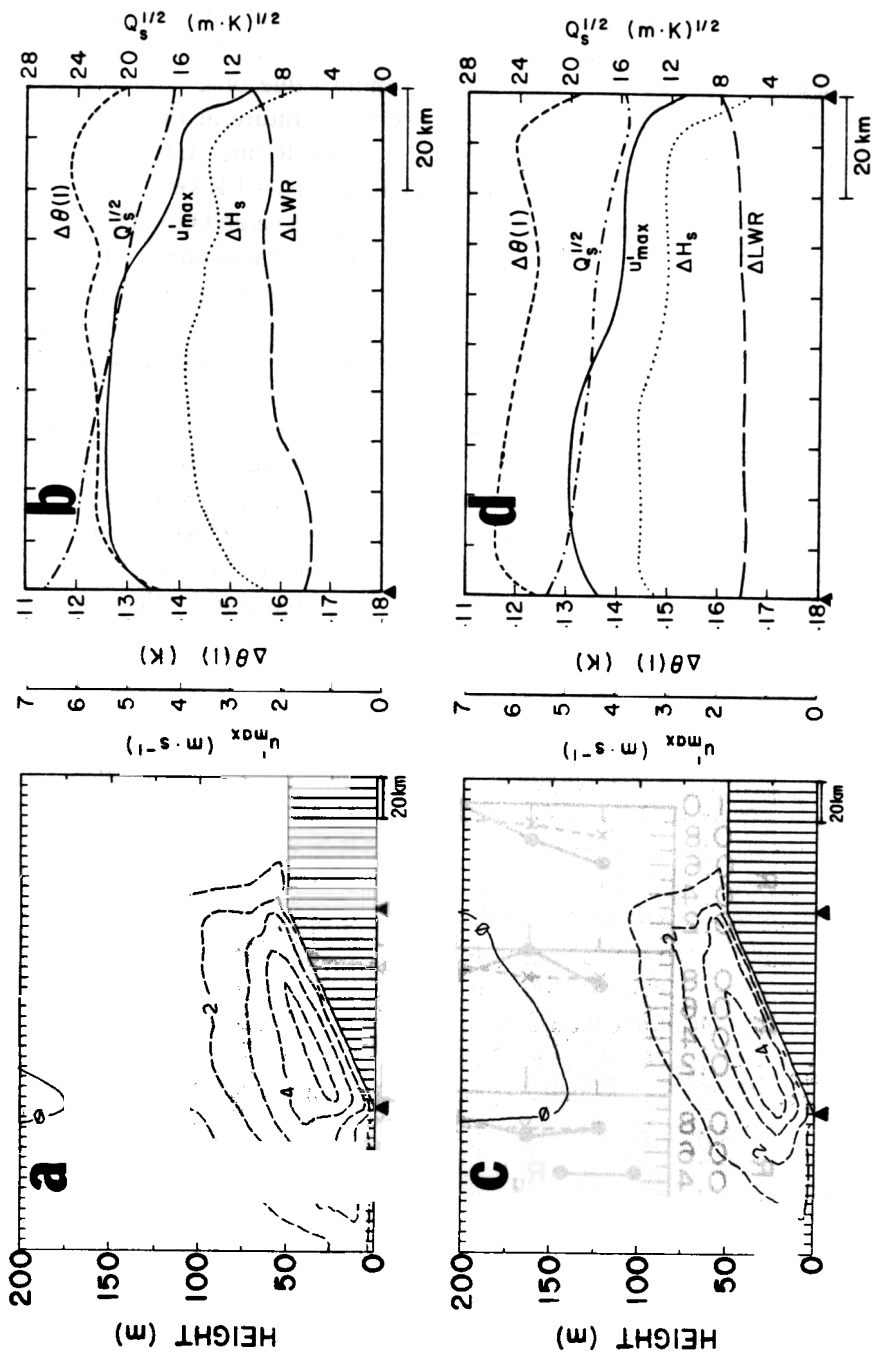

Fig. 6. Case 2b ($H = 500$ m; $\alpha = 0.28°$) (a) vertical cross-section presenting the simulated downslope flow component u' (m s^{-1}) at 0200 LST, $\beta_0 = 1$ K km^{-1}; (b) the variation along the slope portion of the domain at 0200 LST with $\beta_0 = 1$ K km^{-1} of: ΔLWR, ΔH_s, u'_{max}, $Q_s^{1/2}$ and $\Delta\theta(1)$; (c) and (d) the same as (a) and (b) respectively, except for $\beta_0 = 10$ K km^{-1}.

Figure 6 presents several downslope flow characteristics along the slope portion of the simulated domain at 0200 LST (when the flow is nearly steady, $\alpha = 0.28°$). With $\beta_0 = 1\,\mathrm{K\,km^{-1}}$, the vertical flow structure shows uniformity along most of the slope excluding the bottom and top sections (Figure 6a). Similar horizontal uniformity is found also for u'_{max} (i.e., the maximum value of u' above a given grid point), $\Delta\theta(1)$ (the deviation of the potential temperature at the first model level (3.5 m) from the initial temperature), $Q_s^{1/2}$, ΔLWR and ΔH_s. With $\beta_0 = 10\,\mathrm{K\,km^{-1}}$, similar qualitative features are found as with $\beta_0 = 1\,\mathrm{K\,km^{-1}}$. The wind speed maximum values are almost unaffected (see Figures 6a and 6c). The magnitude of $\Delta\theta(1)$ and ΔH_s for $\beta_0 = 10\,\mathrm{K\,km^{-1}}$ are nearly the same as for $\beta_0 = 1\,\mathrm{K\,km^{-1}}$. However, the magnitude of ΔLWR is reduced somewhat, resulting in the decrease in the depth of downslope flow.

Figure 7 presents the time dependence of the ratio of $u'_{max}(\beta_{10})/u'_{max}(\beta_1) = R_{u'}$, and the ratio of $Q_s^{1/2}(\beta_{10})/Q_s^{1/2}(\beta_1), = R_Q$, for the simulations with a plateau height H of 250, 500, and 1000 m, where $\beta_{10} = 10\,\mathrm{K\,km^{-1}}$ and $\beta_1 = 1\,\mathrm{K\,km^{-1}}$. The values of $Q_s^{1/2}$ for the β_{10} case were about 0.75 to 0.90 of the corresponding $Q_s^{1/2}$ values in the β_1 case. The maximum downslope flow u'_{max} for β_{10} was about 0.8 to 0.9 times its values in the β_1 case for the different plateau height simulations, showing that the impact of β_0 on u'_{max} is nearly the same as the impact of β_0 on $Q_s^{1/2}$; viz., the value of u'_{max} is proportional to $Q_s^{1/2}$, as suggested by the analytical solution (Equation 9a).

Normalized downslope flow profiles (i.e., $u' \cdot Q_s^{-1/2}$) in the middle of the three slopes while considering different β_0 values (Figure 8) indicate that, in general,

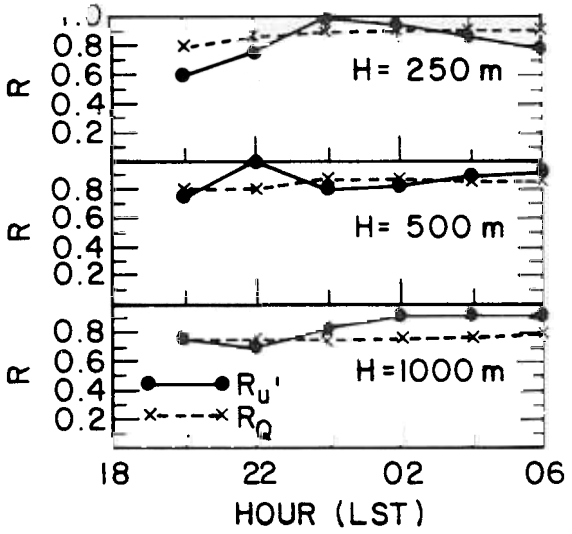

Fig. 7. Time dependence of the ratio, R, of (i) the maximum downslope flow u'_{max}, and (ii) $Q_x^{1/2}$, as computed for $\beta_0 = 10\,\mathrm{K\,km^{-1}}$ and $\beta_0 = 1\,\mathrm{K\,km^{-1}}$ (denoted $R_{u'}$ and R_Q, respectively), for plateau heights of 250, 500, and 1000 m (Case 2).

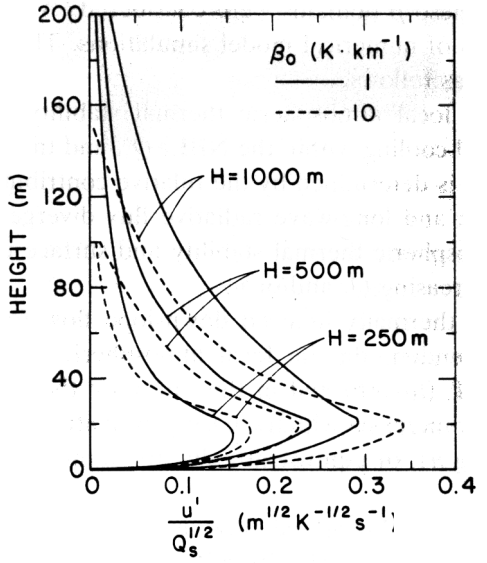

Fig. 8. Numerical model simulated vertical profiles of $u' \cdot Q_s^{-1/2}$ at the middle of the slope at 0200LST (Case 2), for the indicated plateau height and β_0 values.

the profiles for $\beta_0 = 1\,\mathrm{K\,km^{-1}}$ and $10\,\mathrm{K\,km^{-1}}$ are similar for the three plateau height situations. Thus, Figure 8 furthermore supports the analytical result that downslope flow is independent of β_0 and that the downslope flow is proportional to $Q_s^{1/2}$. Figure 8 shows that the depth of the layer which contains most of the downslope flow kinetic energy is not sensitive to the change in β_0 (the result appears to be valid at least when the slope steepness is relatively small). This feature is in agreement with results obtained in Case 1 (Fig. 4a).

In conclusion, when all the model input parameters are kept unchanged (except for β_0), the simulated downslope flow characteristics such as sensible heat flux, the height of the NBL, net LWR flux divergence across the NBL, Q_s, and downslope flow intensity, decrease only mildly with a significant increase of β_0. The impact on downslope flow exerted by changing β_0 can be summarized as follows: significantly increasing β_0 leads to a weakly decreasing Q_s, which consequently results in a small reduction of downslope flow. However, the value of $u'_{\max} \cdot Q_s^{-1/2}$ is essentially independent of β_0.

4. Conclusions

The present study has investigated the impact of background atmospheric thermal stability (external to the NBL) and local atmospheric thermal stability (internal to the NBL), as well as slope steepness, on the nighttime thermally induced downslope flow (assuming negligible synoptic flow). Slope lengths of 20–200 km,

which are typical of meso-β domains were considered. Analytical solutions were compared with results of numerical model simulations. The major conclusions of these evaluations are as follows:

(i) The nighttime local atmospheric thermal stability is dependent on the amount of total cooling within the NBL, Q_s, and the stratification index n. The value of n is determined by the relative contributions of sensible heat flux divergence and long-wave radiative flux divergence across the NBL. The local atmospheric thermal stability and surface inversion strength increase with increasing Q_s and/or n.

(ii) The nighttime thermally induced downslope flow for a given NBL total cooling is dependent on the local atmospheric thermal stability profile within the NBL (as reflected in this study by the stability index n). The downslope flow increases with increasing local atmospheric thermal stability (i.e., increasing n), or equivalently due to an increase in surface inversion strength.

(iii) Thermally induced downslope flow as a function of a non-dimensional vertical coordinate is essentially independent of background atmospheric thermal stability, when other parameters remain unchanged.

(iv) Selected numerical model simulations suggest that the intensity of downslope flow u', for low slope steepness, is proportional to $(\sin \alpha)^{1/2}$. These simulations indicate a decrease in n (i.e., an increase of the relative contribution of turbulent sensible heat flux divergence, as contrasted with long-wave radiational cooling) with slope steepness.

(v) Analytical and numerical model evaluations are in general agreement for the several cases simulated in the present study.

Acknowledgements

This study was supported by the NSF under Grant # ATM-8616662 and the NPS under contract NA81RAH00001, Amendment 17, Item 15. The computations were carried out by the NCAR Facility (NCAR is supported by the NSF). Douw Steyn and anonymous reviewers provided useful comments on the manuscript. We would like to thank Dallas McDonald, Bryan Critchfield, and Shawn Rios for the preparation of the manuscript, and Ken Streeb for drafting the figures.

Appendix. Parameterization the Nocturnal Eddy Exchange Coefficient

Following Blackadar (1979), the eddy exchange coefficient in the nocturnal stable boundary layer can be expressed as locally dependent on stability according to:

$$K = 1.1l^2 S\left[1 - \frac{\mathrm{Ri}}{\mathrm{Ri}_c}\right], \quad R_i < \mathrm{Ri}_c \tag{A1}$$

$$\mathrm{Ri} = \lambda \frac{\partial\theta/\partial z}{S^2}$$

Here Ri_c is the critical Richardson number, which is equal to 0.25 for infinitesimal thin layers (e.g., see Arya, 1972), $l = k_0 z/\varphi$, k_0 is the von Karman constant, $S = [(\partial u/\partial z)^2 + (\partial v/\partial z)^2]^{1/2}$ is the vertical wind shear, and $\varphi = 1 + 5\xi\zeta$, $\zeta = h/L = bn$, $\xi = z/h$, where L is the Monin-Obukhov stability length and b is a proportionality constant.

Since the extensive data collected during ASCOT (see Dickerson and Gudiksen, 1983) showed that significant downslope flows did not occur when $\mathrm{Ri} < 0.2$, and there was no downslope flow at all when $\mathrm{Ri} < 0.15$, it is reasonable to assume the existence of a near-critical bulk Richardson number, across a NBL in which the downslope flow is well developed (e.g., Nieuwstadt and Tennekes, 1981 for the NBL over horizontal terrain),

Using Equations (2c), (5a), and (A2), the following formulation for S is obtained,

$$S = \left(\frac{\lambda}{\mathrm{Ri}}\frac{\partial\theta}{\partial z}\right)^{1/2} = \left[\frac{n\lambda\Delta\theta}{h\,\mathrm{Ri}}(1-\xi)^{n-}\right]^{1/2}$$

$$\left(\frac{An(n+1)\lambda Q_s}{\mathrm{Ri}\,h^2}\right)^{1/2} - \xi)^{(n-1)/2}$$

where A is defined by Equation (5b).

Substituting (A3) into (A1) results in an expression for the eddy exchange coefficient K:

$$K(\xi) = A' h Q_s^{1/2} f_2(\xi, \zeta)\,,$$

where

$$A' = 1k_0^2[An(n+1)\lambda]^{1/2} \tag{A5}$$

and

$$\frac{\xi^2(1-\xi)^{(n-1)/2}}{(1+5\zeta\xi)^2}\left(\frac{1-\mathrm{Ri}/\mathrm{Ri}_c}{\mathrm{Ri}^{1/2}}\right)$$

In fact, $\mathrm{Ri} \approx$ constant over a wide range of ζ within the NBL (e.g., Nieuwstadt, 1985), so the term $(1 - \mathrm{Ri}/\mathrm{Ri}_c)\mathrm{Ri}^{-1/2} \rightarrow$ constant.

Equation (A4) suggests that the eddy exchange coefficient with the NBL is proportional to h and $Q_s^{1/2}$. Here Q_s is a measurement of the buoyancy force over the slope since the total buoyancy force over the NBL, $\int_0^h \lambda\theta' \sin\alpha\, dz$, equals $\lambda Q_s \sin\alpha$; and h reflects the depth of atmospheric turbulence within the NBL. Therefore, h increases with an increase in turbulence intensity (see similar model results reported in Dickerson, 1980). Equation (A4) also indicates that $K = 0$ at

$\xi = 0$ and $\xi = 1$. Equation (A4) is similar to that given by Brost and Wyngaard (1978), viz.,

$$K = k_0 u_* h f_3(\xi, \zeta) . \tag{A7}$$

This form, in which u_* is present, is consistent with (A4) when we assume the existence of a critical (or near-critical) bulk Richardson number across a well developed NBL or drainage flow (e.g. Nieuwstadt and Tennekes, 1981 for flat terrain). Thus we may write

$$\mathrm{Ri}_b \approx \frac{\lambda h \Delta\theta}{U^2}$$

where

$$h\Delta\theta \approx \bar{c} U^2$$

with $\bar{c} \approx$ constant. Equation (A4) becomes, with the use of Equation (5a),

$$\begin{aligned} K(\xi) &\approx \frac{A' h}{[A(n+1)]^{1/2}} (h\Delta\theta)^{1/2} f_2(\xi, \zeta) \\ &\approx \frac{A'}{[A(n+1)]^{1/2}} \bar{c}^{1/2} U h f_2(\xi, \zeta) \\ &\approx \alpha u_* h f_2(\xi, \zeta) , \end{aligned} \tag{A9}$$

where $u_* = C_D{}^{1/2} U$, C_D being a drag coefficient dependent upon stability, and $\alpha = A'/[A(n+1)C_D]^{1/2}$. It is thus evident that Equation (A9) is of the same form as Equation (A4).

K_0 in Equation (8) is defined by simplifying Equation (A4), with

$$K_0 = n^{-1/2} \int_0 A' f_2(\xi, \zeta) \, \mathrm{d}\xi \tag{A10}$$

References

Arya, S. P. S.: 1972, 'The Critical Condition for the Maintenance of Turbulence in Stratified Flows', *Quart. J. Roy. Meteorol. Soc.* **98**, 264–273.

André, J. C. and Mahrt, L.: 1982, 'The Nocturnal Surface Inversion and Influence of Clear-air Radiative Cooling', *J. Atmos. Sci.* **39**, 864–878.

Blackadar, A. K.: 1979, 'High Resolution Models of the Planetary Boundary Layer', in J. Pfafflin and E. Ziegler (eds.), *Advances in Environmental Science and Engineering* **1** Gordon and Breach, pp. 50–85.

Brost, R. A. and Wyngaard, J. C.: 1978, 'A Model Study of the Stable Stratified Planetary Boundary Layer, *J. Atmos. Sci.* **35**, 1427–1440.

Dickerson, M. H. (ed.): 1980, *A Collection of Papers Based on Drainage Wind Studies in the Geysers Area of Northern California: Part I*, UCID-18884, ASCOT-80-7, 22 chapters.

Dickerson, M. H. and Gudiksen, P. H. (Eds.): 1983, 'Atmospheric Studies in Complex Terrain', Technical Progress Report FY-1979 through FY-1983. Lawrence Livermore National Laboratory, UCID-19851, ASCOT84-1, 367 pp.

Doran, J. C. and Horst, T. W.: 1983, 'Observations and Models of Simple Nocturnal Slope Flows', *J. Atmos. Sci.* **40**, 708–717.

Ellison, T. H. and Turner, J. S.: 1959, 'Turbulent Entrainment in Stratified Flows', *J. Fluid Mech.*, **6**, 423–448.

Garratt, J. R. and Ryan, B. F.: 1989, 'The Structure of the Stable Stratified Internal Boundary Layer in Offshore Flow over the Sea', *Boundary Layer Meteorol.* **47**, 17–40.

Kondo, H.: 1984, 'The Difference of the Slope Wind Between Day and Night', *J. Meteorol. Soc. Japan* **62**, 224–232.

Mahrer, Y. and Pielke, R. A.: 1977, 'A Numerical Study of the Air Flow over Irregular Terrain', *Contrib. Atmos. Phys.* **50**, 98–113.

Manins, P. C. and Sawford, B. L.: 1979a, 'Katabatic Winds: A Field Case Study', *Quart. J. Roy. Meteorol. Soc.* **105**, 1011–1025.

Manins, P. C. and Sawford, B. L.: 1979b, 'A Model of Katabatic Winds', *J. Atmos. Sci.* **36**, 619–630.

McNider, R. T. and Pielke, R. A.: 1981, 'Diurnal Boundary-Layer Development over Sloping Terrain', *J. Atmos. Sci.* **38**, 2198–2212.

McNider, R. T. and Pielke, R. A.: 1984, 'Numerical Simulation of Slope and Mountain Flow', *J. Climate Appl. Meteorol.* **23**, 1441–1453.

Nappo, C. J. and Rao, K. S.: 1987, 'A Model Study of Pure Katabatic Flows', *Tellus* **39A**, 61–71.

Nieuwstadt, F. T. H.: 1985, 'A Model for the Stationary, Stable Boundary Layer', in J. C. R. Hunt (ed.), *Turbulence and Diffusion in Stable Environment*, Clarendon Press, Oxford, pp. 149–179.

Nieuwstadt, F. T. H. and Tennekes, H.: 1981, 'A Rate Equation for the Nocturnal Boundary-Layer Height', *J. Atmos. Sci.* **38**, 1418–1428.

Pielke, R. A.: 1974, 'A Three-Dimensional Numerical Model of the Sea Breezes over South Florida', *Mon. Wea. Rev.* **102**, 115–239.

Prandtl, L.: 1942, 'Fuehrer durch die Stromunglehre. Braunschweig', Viewing und Sohn, 382 pp.

Rao, K. S. and Snodgrass, H. F.: 1981, 'A Non-Stationary Nocturnal Drainage Flow Model', *Boundary Layer Meteorol.* **20**, 309–320.

Segal, M., Mahrer, Y., and Pielke, R. A.: 1982, 'Application of a Numerical Mesoscale Model for Determining Persistent Regional Climatological Patterns', *J. Appl. Meteorol.* **21**, 1754–1762.

Yamada, T.: 1979, 'Prediction of the Nocturnal Surface Inversion Height', *J. Appl. Meteorol.* **18**, 526–531.

Yasuda, N., Kondo, J., and Sato, T.: 1986, 'Drainage Flow Observed in a V-shaped Valley', *J. Meteorol. Soc. Japan* **64**, 283–301.